A High Order, Finite Volume, Multilevel WENO Scheme Applied to Porous Media

Todd Arbogast[0000−0001−9692−5478]

Abstract We describe a novel and general framework for solving advection-diffusion equations using finite volume weighted essentially non oscillatory (WENO) techniques on general computational meshes. Such techniques are able to handle advective and (degenerate) diffusive behavior, even when the solution develops shocks or steep fronts. We discuss a robust procedure for producing accurate stencil polynomial approximations and a recently developed multilevel WENO (ML-WENO) reconstruction. It combines stencil polynomials of various degrees (e.g., more than two degrees and including constant polynomials) defined on any set of stencils (e.g., not hierarchically arranged). The nonlinear weighting biases the reconstruction away from both inaccurate oscillatory polynomials crossing a shock or steep front and smooth polynomials of low degree, thereby selecting the smooth polynomial(s) of maximal degree of approximation. We apply these ideas to develop a preliminary finite volume scheme for solving two-phase flow in porous media modeled by Richards equation. Numerical tests of rainwater infiltration show the advantages of using higher order finite volume methods and multilevel WENO reconstructions.

1 Introduction

Discontinuous Galerkin (DG) and finite volume (FV) methods are popular choices for the approximation of advection-diffusion equations

$$u_t + \nabla \cdot [f(u) - D(u)\nabla u] = q(u) \tag{1}$$

for the unknown $u(\mathbf{x},t)$, especially when the equation is advection dominated (i.e., D is small). The pure advection equation (i.e., $D = 0$) often has solutions exhibiting

Todd Arbogast
The University of Texas at Austin, Oden Institute C0200, Austin, Texas, 78712, USA, e-mail: arbogast@oden.utexas.edu

discontinuities. Numerical methods must carefully approximate the solution on the interfaces between mesh cells or elements. DG places many degrees of freedom (DoFs) inside each mesh element E to understand the solution behavior on ∂E, while FV places one DoF inside each mesh element, and looks outside E to determine the behavior of the solution on ∂E.

FV methods have many advantages; we mention three. First, they use only one degree of freedom per mesh element in any space dimension and for any degree of approximation. Second, they maximize the mesh resolution. That is, compared to finite element and DG methods using a similar number of DoFs, the mesh is significantly finer for FV methods. This is important is some applications, such as porous media, where permeability and porosity are generally taken to be constant on each mesh element. Third, the mesh needs no special properties.

In this paper, we discuss a FV scheme approximating (1) involving a recently introduced weighted essentially non-oscillatory (WENO) technique [1]. We then give a preliminary application to Richards equation, which arises in the field of hydrology.

2 The Finite Volume Framework

Let $\mathcal{T}_h$ be a quasi-uniform computational mesh of elements of maximal diameter $h > 0$ over the domain $\Omega \subset \mathbb{R}^d$. We will take $d = 2$ in this paper, but the ideas extend to higher dimensions. The average of $u(\mathbf{x}, t)$ over the mesh element $E \in \mathcal{T}_h$ is

$$\bar{u}_E(t) = \frac{1}{|E|} \int_E u(\mathbf{x}, t)\, d\mathbf{x}\,, \tag{2}$$

where $|E|$ is the area of E. The differential equation (1) can be averaged over E as well. After applying the Divergence Theorem, we find

$$\bar{u}_{E,t} + \frac{1}{|E|} \int_{\partial E} \big(f(u) - D\nabla u\big) \cdot \nu_E \, dS(\mathbf{x}) = \frac{1}{|E|} \int_E q(u)\, d\mathbf{x}\,. \tag{3}$$

A numerical flux function for the advective term is needed both to stabilize computations by adding numerical diffusion and to account for potential discontinuities in the solution. We use the Lax-Friedrichs numerical flux

$$\hat{f}_E(u^-, u^+) = \frac{1}{2}\Big[\big(f(u^-) + f(u^+)\big) \cdot \nu_E - \alpha_{\mathrm{LF}}(u^+ - u^-)\Big]\,, \tag{4}$$

where u^- and u^+ are left and right limits of the solution at the interface ∂E and $\alpha_{\mathrm{LF}} = \max_u \big|\partial f/\partial u\big|$ is the maximum wave speed. Thus

$$\bar{u}_{E,t} + \frac{1}{|E|} \int_{\partial E} \big[\hat{f}_E(u^-, u^+) - D(u)\nabla u \cdot \nu_E\big] dS(\mathbf{x}) = \frac{1}{|E|} \int_E q(u)\, d\mathbf{x}\,. \tag{5}$$

We approximate time evolution using a standard Runge-Kutta method at time levels $0 = t^0 < t^1 < t^2 < \cdots$, so that $\bar{u}_E^n \approx \bar{u}_E(t^n)$ for each $n > 0$. We also need to approximate $u^{\pm}(\mathbf{x})$ and $D(u)\nabla u \cdot \nu_{E_0}(\mathbf{x})$ on ∂E_0 for each $E_0 \in \mathcal{T}_h$, given only the $\bar{u}_E$.

3 Construction of Stencil Polynomials

Given a mesh stencil $S = \{E_j \in \mathcal{T}_h, \text{ some } j\}$ of contiguous mesh elements, we can define its stencil polynomial

$$P(\mathbf{x}) = \sum_{\alpha<r} c_\alpha \left(\frac{\mathbf{x} - \mathbf{x}_S}{h_S}\right)^\alpha \tag{6}$$

by matching the averages over each $E \in S$, i.e.,

$$\frac{1}{|E|}\int_E P(\mathbf{x})\, d\mathbf{x} = \bar{u}_E \qquad \Longleftrightarrow \qquad A\mathbf{c} = \mathbf{u}\,, \tag{7}$$

for some $M \times N$ matrix A. This generally requires least-squares fitting [5], since the number of polynomial coefficients N is usually not the number of stencil elements M.

We find the SVD decomposition and the singular values

$$A = U\Sigma V^T\,, \quad s_1 \geq s_2 \geq \cdots \geq s_m\,. \tag{8}$$

If the matrix A^TA is nonsingular ($m = M$), we can solve for the polynomial coefficients $\mathbf{c} = (A^TA)^{-1}A^T\mathbf{u} = V\Sigma^{-1}U^T\mathbf{u}$. However, one actually selects a target element $E_0 \in S$ and constrains $\mathbf{c}$ to match (7) on E_0 [5]. In [1], it was shown how to determine when one obtains a reliable approximation.

Theorem 1 *There is some moderate constant $C \geq 0$ such that for $\mathbf{x} \in E_0$,*

$$|\mathcal{D}^\alpha(u(\mathbf{x}) - P(\mathbf{x}))| \leq Ch^{r-|\alpha|} \quad \forall\, |\alpha| \leq r\,, \tag{9}$$

provided the matrix A^TA is well conditioned and the mesh is quasiuniform.

If the condition number $(s_1/s_M)^2$ is much larger than one (say greater than 10^8), we should reject the stencil polynomial. We could then try to add elements to the stencil, but in dimensions greater than one, it is not clear which elements should be added. Moreover, a larger stencil is undesirable, since it is more likely to cross a shock. An alternative is to decrease the polynomial degree $r - 1$ and try again [1]. This option is practical in multidimensions, and the algorithm will terminate at least with $r = 1$ (i.e., a constant polynomial). In other words, we fix the stencil and find the best polynomial approximation it supports.

We must also reliably detect a shock or steep front. For polynomial $P(\mathbf{x})$ targeting element E_0, its smoothness indicator is σ_P [4]. It satisfies $\sigma_P = D_0h_0^2 + O(h^3)$ if u is smooth on the stencil (for some constant $D_0 \geq 0$), and is $O(1)$ if u has a jump discontinuity on the stencil.

4 ML-WENO Reconstructions

The general philosophy of ENO and WENO reconstructions is that they should involve approximations that do not cross a shock. They do so by considering many stencil polynomials P_ℓ of degree $r_\ell - 1$ for target element $E_0 \in \mathcal{T}_h$ and taking a linear combination

$$R(\mathbf{x}) = \sum_\ell \tilde{\omega}_\ell P_\ell(\mathbf{x}) \,. \tag{10}$$

Most current WENO techniques are unsuitable for general approximation in multidimensions. They require polynomials of only two degrees, or stencils arranged hierarchically. Moreover, they generally require non-constant polynomials. An exception is the multilevel WENO (ML-WENO) reconstruction presented in [1]. Choose *linear weights* $\omega_\ell > 0$ (such as 1, although 10^{-4} is perhaps better for weighting constant polynomials), and then define the *nonlinear weights*

$$\tilde{\omega}_\ell = \frac{\hat{\omega}_\ell}{\sum_k \hat{\omega}_k} \quad \text{where} \quad \hat{\omega}_\ell = \frac{\omega_\ell}{(\sigma_{P_\ell} + \epsilon_0 h^2)^{r_\ell}} \,. \tag{11}$$

Here $\epsilon_0 > 0$ is a small parameter (such as 10^{-2} or 10^{-6}). This weighting selects the stencil polynomials of highest order of accuracy that *do not cross a shock*.

Theorem 2 *There is some $C > 0$ such that for all $\mathbf{x} \in E_0$ (the target element),*

$$|u(\mathbf{x}) - R(\mathbf{x})| \le C h^{r_{\max}} \,, \tag{12}$$

where $r_{\max} = \max_\ell \{r_\ell : u$ is smooth on the ℓth stencil$\}$.

Returning to (5), we use the reconstruction R to evaluate $u^\pm$ on the boundary of the target element E_0. We also evaluate the normal derivative $D(u)\nabla u \cdot \nu_E$ by evaluating R on the line normal to an edge of E_0, interpolating the results, and differentiating the resulting polynomial, as was discussed in [2].

5 Preliminary Application to Richards Equation

As a preliminary investigation of the use of ML-WENO in solving problems in porous media, we consider solving a rainwater infiltration problem. The two-phase air-water system in hydrology is generally governed by Richards equation [3]. The system is modeled assuming that the air phase is infinitely mobile and connected to the surface, so the air pressure is fixed at atmospheric pressure, taken as zero. The unknown solution then consists of only the water saturation s, pressure p_{w}, and velocity $\mathbf{v}_{\mathrm{w}}$. The equations can be written as

$$\phi s_t + \nabla \cdot \mathbf{v}_\mathrm{w} = q(s)\,, \tag{13}$$

$$\mathbf{v}_\mathrm{w} = -\lambda_\mathrm{w}(s)\,K\,(\nabla p_\mathrm{w} - \rho_\mathrm{w}\,\mathbf{g})\,, \tag{14}$$

$$p_\mathrm{c}(s) = -p_\mathrm{w} \le 0\,, \tag{15}$$

where ϕ is the porosity, K is the permeability, λ_w is the relative mobility, ρ_w is the water density, $\mathbf{g}$ is the gravity vector, $p_\mathrm{c}(s)$ is the (macroscopic) capillary pressure function, and q models the external wells appearing in the domain.

We can simplify the system by defining the Kirchhoff Transformation

$$D(s) = -\int_0^s \lambda_\mathrm{w}(S)p_\mathrm{c}'(S)\,dS\,, \tag{16}$$

which implies that

$$\nabla D(s) = -\lambda_\mathrm{w}(s)\nabla p_\mathrm{c}(s) = \lambda_\mathrm{w}(s)\nabla p_w\,. \tag{17}$$

We eliminate $p_\mathrm{w} = -p_\mathrm{c}(s)$ and $\mathbf{v}_\mathrm{w} = -K\nabla D(s) + \rho_\mathrm{w}\,\lambda_\mathrm{w}(s)\,K\,\mathbf{g}$ to obtain the single equation

$$\phi s_t - \nabla \cdot \big(K\nabla D(s)\big) + \nabla \cdot \big(\rho_\mathrm{w}\,\lambda_\mathrm{w}(s)\,K\,\mathbf{g}\big) = q(s)\,. \tag{18}$$

In finite volume form over the mesh element E, the equation is

$$\begin{aligned}\phi\bar{s}_{E,t} - \frac{1}{|E|}\int_{\partial E} K\nabla D(s)\cdot\nu\,dS(\mathbf{x}) \\ + \frac{1}{|E|}\int_{\partial E}\rho_\mathrm{w}\,\lambda_\mathrm{w}(s)\,K\,\mathbf{g}\cdot\nu\,dS(\mathbf{x}) = \frac{1}{|E|}\int_E q(s)\,d\mathbf{x}\,.\end{aligned} \tag{19}$$

The terms on the left hand side model accumulative, (degenerate) diffusive, and advective processes. The third term requires a numerical flux (4).

5.1 Numerical Implementation

We assume a single rock type and a constant porosity, so s is smooth but may exhibit steep fronts. We present a simple algorithm based on advancing the saturation through time.

Time is advanced from t^n to t^{n+1} by an explicit Runge-Kutta method with ℓ_max stages. Set $\bar{s}^{n,0} = \bar{s}^n$. For each stage $\ell = 0, 1, \ldots, \ell_\mathrm{max} - 1$, advancement of $\bar{s}^{n,\ell}$ to $\bar{s}^{n,\ell+1}$ can be represented as

$$\bar{s}^{n,\ell} \xrightarrow{\text{ML-WENO}} R^{n,\ell} \xrightarrow{\text{point evaluation}} (s^{n,\ell}, p_\mathrm{w}^{n,\ell}, \mathbf{v}_\mathrm{w}^{n,\ell}) \xrightarrow{\text{transport}} \bar{s}^{n,\ell+1}\,. \tag{20}$$

The first step in (20) is to use ML-WENO to reconstruct $R^{n,\ell} \approx \bar{s}^{n,\ell}$ over each element of the mesh. The second step uses the reconstructions to find the required point evaluations of $s^{n,\ell}$, $p_\mathrm{w}^{n,\ell}$, and $\mathbf{v}_\mathrm{w}^{n,\ell}$ needed in the approximation of (19). The

third step results in the new value of $\bar{s}^{n,\ell+1}$ after solving the finite volume transport equation (19). Finally, after all Runge-Kutta stages, we set $\bar{s}^{n+1} = \bar{s}^{n,\ell_{\max}}$.

We have chosen to reconstruct the saturation. However, we should expect that reconstruction of $p_{\rm w}$ would be more accurate than reconstruction of s, since in general the variable $p_{\rm w}$ is smoother than s. If we did so, we would need to take the finite volume unknowns to be $\bar{p}^n_{{\rm w},E}$. The advancement of $\bar{p}^{n,\ell}_{\rm w}$ to $\bar{p}^{n,\ell+1}_{\rm w}$ would then require an additional step, which would follow the procedure

$$\begin{aligned}\bar{p}^{n,\ell}_{\rm w} \xrightarrow{\text{ML-WENO}} R^{n,\ell} \xrightarrow{\text{point evaluation}} (s^{n,\ell}, p^{n,\ell}_{\rm w}, \mathbf{v}^{n,\ell}_{\rm w}) \\ \xrightarrow{\text{transport}} \bar{s}^{n,\ell+1} \xrightarrow{\text{transform}} \bar{p}^{n,\ell+1}_{\rm w}\,.\end{aligned} \tag{21}$$

The approximation of the differential equation (19) would still lead to transport of $\bar{s}^{n,\ell+1}$ on each element, and these would need to be transformed into values for $\bar{p}^{n,\ell+1}_{\rm w}$ on each element. It is an open problem as to how to effectively define this transformation while maintaining accuracy.

5.2 Numerical Test of Water Infiltration

We consider a 100 m × 10 m groundwater domain with continuous infiltration of water on a portion of the top boundary, as shown in Figure 1. The initial saturation is otherwise in gravitational equilibrium. The figure also shows the heterogeneous permeability, which varies from about 0.1 to 1 Darcy. We use van Genuchten capillary pressure and water mobility curves as shown in Figure 2.

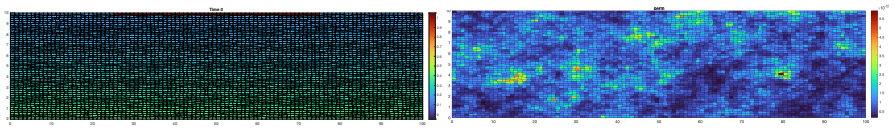

Initial saturation Absolute permeability (in m^2)

Fig. 1 The groundwater domain, showing the initial saturation $s(\mathbf{x}, 0)$ and absolute permeability K.

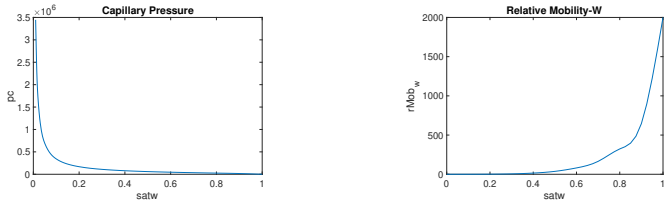

Fig. 2 The van Genuchten capillary pressure $p_{\rm c}$ (in MKS units) and water mobility curves $\lambda_{\rm w}$.

We impose a 100×50 mesh of quadrilaterals over the domain (see Figure 1). We use the explicit forward Euler time stepping method, although the third order explicit SSP Runge-Kutta method gives similar results. The time step is taken to be $\Delta t = 0.001$ days, and we compute 6000 steps (6 days).

We show the results of using low order methods in Figure 3. Displayed is the saturation at times 0.2, 1, 2, 4, and 6 days. The ML-WENO(1) method simply uses a constant polynomial over each target element as the reconstruction, and amounts to a standard first order accurate upwind finite volume method. The ML-WENO(2,1) method combines a linear polynomial defined over a stencil of five elements sharing an edge with the target element, and a constant polynomial; that is, it is second order in smooth regions but drops to first order near a steep front. These two results are fairly similar. Not shown are the results using ML-WENO(3,1), which are similar to the other two. The quadratic polynomial in ML-WENO(3,1) is defined on a stencil of nine elements that share a vertex with the target element. These three methods all drop to first order near the steep front, which limits the accuracy of the solution.

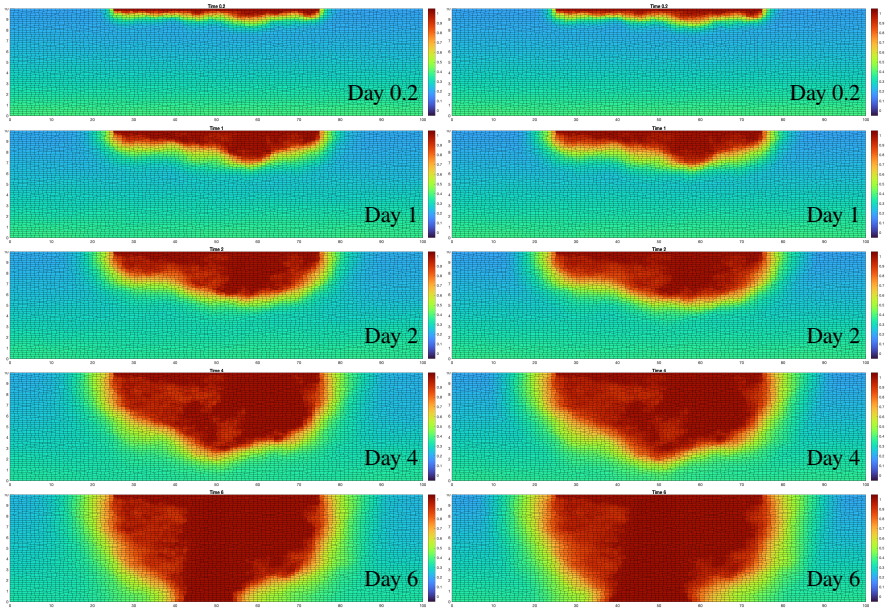

Fig. 3 Saturation computed using the ML-WENO(1) and ML-WENO(2,1) reconstructions.

The results of using third order methods is shown in Figure 4. The ML-WENO(3,2) and ML-WENO(3,2,1) results are similar to each other, but differ significantly from the low order methods. The third order methods show a sharper front and a faster infiltration of water. Near the steep front, the ML-WENO(3,2) method drops to a linear approximation, while the three level, ML-WENO(3,2,1) method usually drops to a linear approximation but sometimes to a constant approxima-

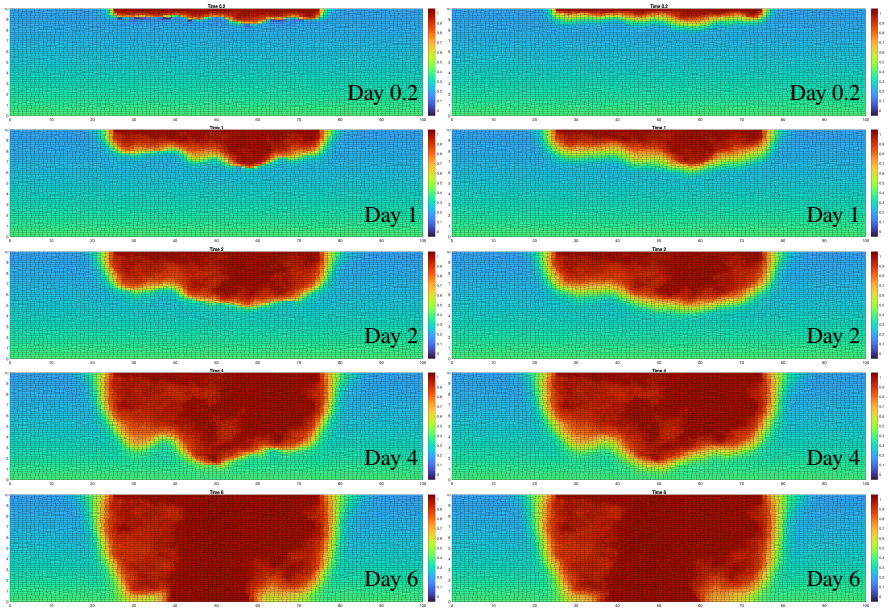

Fig. 4 Saturation computed using the ML-WENO(3,2) and ML-WENO(3,2,1) reconstructions.

tion (the relative linear weight for the constant polynomial is taken to be 10^{-4} for ML-WENO(3,2,1)). Overall, ML-WENO(3,2) gives a bit sharper front, but it also displays some undershoot, as can be seen at 0.2 and 1 day. Adding the constant polynomials into the reconstructions alleviates this problem.

Competing Interests This study was funded by U.S. National Science Foundation grant DMS-1912735. The author has no conflicts of interest that are relevant to the content of this chapter.

References

1. Arbogast, T., Huang, C.S., Tian, C.: A finite volume multilevel WENO scheme for multidimensional scalar conservation laws. Submitted (2023)
2. Arbogast, T., Huang, C.S., Zhao, X.: Finite volume WENO schemes for nonlinear parabolic problems with degenerate diffusion on non-uniform meshes. J. Comput. Phys. **399**(108921) (2019). DOI 10.1016/j.jcp.2019.108921
3. Bear, J., Cheng, A.H.D.: Modeling Groundwater Flow and Contaminant Transport. Springer, New York (2010)
4. Friedrich, O.: Weighted essentially non-oscillatory schemes for the interpolation of mean values on unstructured grids. J. Comput. Phys. **144**, 194–212 (1998)
5. Harten, A., Chakravarthy, S.R.: Multi-dimensional ENO schemes for general geometries. Tech. Rep. 91–76, Institute for Computer Applications in Science and Engineering, NASA Langley Research Center, Hampton, Virginia (1991). Contract No. NAS1-18605